Algebraic Nonlocal Transition Modeling of Laminar Separation Bubbles Using k–ω Turbulence Models

Luis Bernardos, François Richez, Vincent Gleize, Georges Gerolymos

Algebraic Nonlocal Transition Modeling of Laminar Separation Bubbles using k-ω Turbulence Models

Luis Bernardos[1], F. Richez[2] and V. Gleize[3]
ONERA, Meudon, 92190, France

G.A. Gerolymos[4]
Sorbonne Université, 75005 Paris, France

Algebraic transitional extensions for the accurate computation of laminar separation bubbles are developed for use with k-ω models. The transitional model, based on integral boundary-layer parameters and transition criteria, introduces streamwise-variable weighting of the production terms in the k-ω equations and delay of the shear-stress-limiter activation. Calibration to fit available DNS data yields satisfactory results for a flat-plate reference case, both for skin-friction and velocity-profiles. It is shown that the model can be adapted to different k-ω variants by appropriate calibration of coefficients. The model is then validated for 2 airfoil test-cases, both for very low and higher Reynolds numbers, a NACA 0012 airfoil at chord-based Reynolds number $Re_c = 10^5$ and angle-of-attack $\alpha = 10.55\,\mathrm{deg}$ and a S809 airfoil at $Re_c = 2 \times 10^6$ and $\alpha = 1\,\mathrm{deg}$. For both application cases comparison with available data is satisfactory.

Nomenclature

c	=	airfoil chord length (m)
C_{lim}	=	shear-stress limiter delay function
C_p	=	pressure coefficient

[1] PhD Student, Aerodynamics, Aeroelasticity and Acoustics Department. luis.bernardos_barreda@onera.fr
[2] Research Scientist, Aerodynamics, Aeroelasticity and Acoustics Department. francois.richez@onera.fr
[3] Research Scientist, Aerodynamics, Aeroelasticity and Acoustics Department. vincent.gleize@onera.fr
[4] Professor, Faculty of Science and Engineering, 4 place Jussieu, Senior Member AIAA. georges.gerolymos@sorbonne-universite.fr

c_f = skin-friction coefficient

F_2 = Menter's second blending function

f^{tr} = Transition function

H = boundary-layer shape parameter ($= \delta^*/\theta$)

k = turbulence kinetic energy ($\mathrm{m}^2\ \mathrm{s}^{-2}$)

k_L = laminar kinetic energy ($\mathrm{m}^2\ \mathrm{s}^{-2}$)

M = Mach number

N = total amplification factor

N_{cr} = critical total amplification factor

n = airfoil wall-normal coordinate (m)

$\mathcal{P}_k$ = production of turbulence kinetic energy ($\mathrm{kg\ m}^{-1}\ \mathrm{s}^{-3}$)

p = static pressure (Pa)

Re_c = chord-based Reynolds number, $\rho_e\, c\, U_e/\mu_e$

Re_θ = momentum-thickness Reynolds number, $\rho_e\, \theta\, U_e/\mu_e$

S_{ij} = strain rate tensor (s^{-1})

s = wall-tangent curvilinear abscissa (m)

s_sep = laminar separation point (m)

s_tr = transition onset (m)

$\widehat{s}$ = Dimensionless streamwise abcissa, $(s - s_\mathrm{tr})/(s_\mathrm{tr} - s_\mathrm{sep})$

$\widehat{s}_a$, $\widehat{s}_b$, $\widehat{s}_c$, a = Transitional model closure coefficients

T_u = turbulence intensity, $(2k/3)^{1/2}/U_e$

$\overline{u_i}$ = local Reynolds-averaged velocity i-component ($\mathrm{m\ s}^{-1}$)

u_s = velocity component projected into s abscissa ($\mathrm{m\ s}^{-1}$)

u_τ = friction velocity, $(\tau_w/\rho)^{1/2}$ ($\mathrm{m\ s}^{-1}$)

u^+ = velocity in wall-units, u/u_τ

U_e = boundary-layer edge velocity ($\mathrm{m\ s}^{-1}$)

x = DNS wall-tangent coordinate (m)

x^R = DNS turbulent reattachment point (m)

x^S = DNS laminar separation point (m)

x_{RS} = Dimensionless DNS coordinate frame, $(x - x^R)/(x^R - x^S)$

y = DNS wall-normal coordinate (m)

y^+ = distance in wall-units, $\rho u_\tau y/\mu$

α = airfoil's angle of attack (deg)

α_ω = turbulence model's production of ω closure coefficient

β_k, β_ω = turbulence model's dissipation of k and ω closure coefficients

γ = Intermittency factor

δ = boundary-layer thickness (m)

δ^* = boundary-layer displacement thickness (m)

ε = dissipation of turbulence kinetic energy ($m^2\ s^{-3}$)

θ = boundary-layer momentum thickness (m)

Λ_2 = Pohlhausen parameter

μ = molecular dynamic viscosity (kg $m^{-1}\ s^{-1}$)

μ_t = dynamic eddy viscosity (kg $m^{-1}\ s^{-1}$)

ν = molecular kinematic viscosity ($m^2\ s^{-1}$)

ν_t = kinematic eddy viscosity ($m^2\ s^{-1}$)

ρ = density (kg m^{-3})

σ_k, σ_ω, σ_d = turbulence model's Prandtl diffusion coefficients for k, ω, and the cross-diffusion.

τ_w = wall shear stress (kg $m^{-1}\ s^{-2}$)

Ω_{ij} = Rotation-rate tensor (s^{-1})

ω = Turbulence specific dissipation rate (s^{-1})

I. Introduction

Laminar separation bubbles [1, LSBs] appear in numerous aerodynamic applications, such as dynamic stall phenomenon of helicopter blades [2, 3], low-Reynolds number micro air-vehicles (MAV) [4] or wind turbines with enhanced laminarity [5]. It is well established that the flow initially undergoes laminar separation because of the adverse pressure-gradient [6], followed by transition onset in the separated shear-layer [7], identified as the amplification of Kelvin-Helmholtz instabilities leading to turbulence [8] . Increased turbulent mixing in the shear layer may, depending on flow conditions [9], lead to rapid reattachment (short bubble locally modifying wall-pressure distribution [1]) or remain separated for longer distances (long bubble globaly modifying wall-pressure distribution [1]). In both cases, airfoil lift, drag and moment are influenced by the presence of the bubble.

RANS (Reynolds-averaged Navier-Stokes) turbulence models require specific transition information and/or modification to handle the separation-induced transition which dominates the flow [7, 10]. Numerous early [1, 6, 9, 11, 12] and more recent [8, 13–15] studies, both experimental and computational, highlight the complex physics of the transitional flow inside laminar separation bubbles (LSBs), such as pronounced three-dimensionality, high unsteadiness, turbulent breakdown driven by multiple coherent structures and complex oscillator and amplifier instability mechanisms that may lead to notable changes in the flow topology. Several approaches of varying degree of empiricism have been used to predict this difficult flow.

Ultimately, improved transport-equation based transition models [16] are expected to accurately predict such flows. Correlation-based models [17, 18] reformulate widely used transition correlations [19] into coefficients of transport equations for the intermittency [20, 21] and other transition parameters, to obtain local, and recently [22] Galilean invariant, transition models. Physics-based models [23–25] generally rely on the concept [26] of laminar (pre-transitional) kinetic energy $k_{\mathrm{L}} \approx \frac{1}{2}\overline{u'^2}$ (essentially streamwise, in agreement with transition physics [27] and with the observed rapid increase of the Reynolds-stress tensor anisotropy in very low Reynolds number channel flows [28]), which is computed by a specific transport equation, to trigger and control transition in the turbulence model. Transport-equation based transition models are quite successful in mimicking transitional flow effects and in detecting transition [16]. Given the extreme difficulty of accurately predicting transition, algebraic nonlocal transition models are also developed [29], including specific adaptations of additional transport equations [30–32].

Numerous authors have contributed to RANS modeling of LSBs on airfoils, especially at low chord-based Reynolds number Re_c. Yuan *et al.* [33] and Windte *et al.* [34] performed extensive RANS modeling of LSBs for the flow around a SD7003 airfoil at Re_c =60,000, with various models, and concluded that Menter's BSL [35] k-ω performed quite well. Source terms were disabled in the laminar regions upstream of transition onset which was determined using an approximate envelope method [34]. Lian and Shyy [36] proposed a nonlocal intermittency model for the activation of Wilcox's 1994 k-ω [37], through direct weighting of the eddy viscosity $\nu_t^{\mathrm{effective}} = \nu_t\gamma$, and determined transition onset by the e^N method [38]. Calculations of the SD7003 airfoil at $Re_c = 60,000$ at

various angles of attack gave promising results [36]. The same flow was studied by Catalano and Tognaccini [39] with disabled source terms in the laminar regions upstream of the user-prescribed transition onset. These authors proposed a modification of the F_2 blending function appearing in the expression of the shear limiter of Menter's k-ω SST model [35] and of the cut-off value of ω, thus enhancing turbulence production in the transitional region and improving upon the results of the original formulation. An empirical transition onset correlation was added to the method [40] which was applied to various airfoil calculations (SD7003, NACA 0012, S809 and S827). No specific treatment of the transitional region was performed, in the sense that the activation of the turbulence model was made instantly through the source terms at the transition onset.

Despite the encouraging results of the previously described approaches, accurate prediction of LSB is still challenging. As remarked by Dick and Kubacki [16], the quality of the predictions of separation-induced transition remains case-dependent. Numerous existing methods focus on correctly predicting the transition onset, but the transition region prediction still relies on the turbulence model's unapprehended ability to correctly produce turbulence at and downstream of the transition onset. In this paper we develop a transition modeling formulation that intends to account for the turbulence growth within a LSB and in the downstream relaxation flow region. This formulation is based on the observations of Direct Numerical Simulation (DNS) results obtained from a simple flat plate configuration.

We concentrate in this work on linear k-ω models [41, p.124] which are largely used as the underlying RANS framework of transition models [37, 42]. The main focus of the paper is to develop a transitional adaptation of k-ω models, where the transition process in LSBs, from transition onset to fully turbulent flow, is represented with reasonable accuracy. To this purpose, laminar separation transition triggering (hereafter LSTT) in the k-ω model is progressive in the streamwise direction (s), from the criteria-determined [43–45] transition onset (s_{tr}) to full transition. The assumption is made, that the streamwise length between the laminar separation point (s_{sep} which is exactly determined by the solution of the laminar Navier-Stokes equations) and the criteria-determined transition onset, $s_{\mathrm{tr}} - s_{\mathrm{sep}}$, is the characteristic lengthscale of the LSTT-process. Therefore, triggering functions of

the model are expressed in terms of the nondimensional coordinate

$$\hat{s} := \frac{s - s_{tr}}{s_{tr} - s_{sep}} \tag{1}$$

Furthermore, wall-normal variations in the LSTT model are neglected, in line with many algebraic transition models using intermittency functions [36, 46]. The triggering coefficients control the production of k and ω, and hence the growth of turbulence. They are calibrated to obtain the best possible agreement with available LSB DNS data [47, 48]. Although most methods dealing with the transition region use the concept of intermittency [21, 22], the transition-triggering functions used in the present work are not directly related to this concept, but should rather be considered as "*empirical weighting coefficients*" [49] designed to reproduce as best as possible the progressive growth of turbulence in LSBs. Therefore they are not necessarily bounded by 1, but may be designed to locally overshoot this bound.

The present paper is organized as follows. In section II we present the main reference flow of the current study. In section II B we apply some classical RANS approaches to the modeling of the laminar separation bubble, and we highlight the points where there is room of improvement. In section III we propose the new model that improves the predictions of the reference flow. The calibration of the proposed model is presented in section IV. In section V we validate the proposed model for low and high Reynolds number flows around the airfoils NACA 0012 and S809, respectively.

II. DNS calibration database

The proposed model was calibrated using LSB DNS data (§II A), based on the analysis of the performance of existing models (§II B).

A. DNS database

The flow configuration (Fig. 1) consists of a flat-plate with an upper slip-wall (dashed lines) that produces a streamwise variable adverse pressure gradient on the lower no-slip wall (hatched). Upstream of the no-slip wall there is a symmetry condition at the bottom of the domain (dashed-dotted line). Inflow conditions are applied on ① and ②, and an outflow condition on ⓪. The variable adverse pressure gradient induced by the curved upper wall mimics the pressure distribution at the

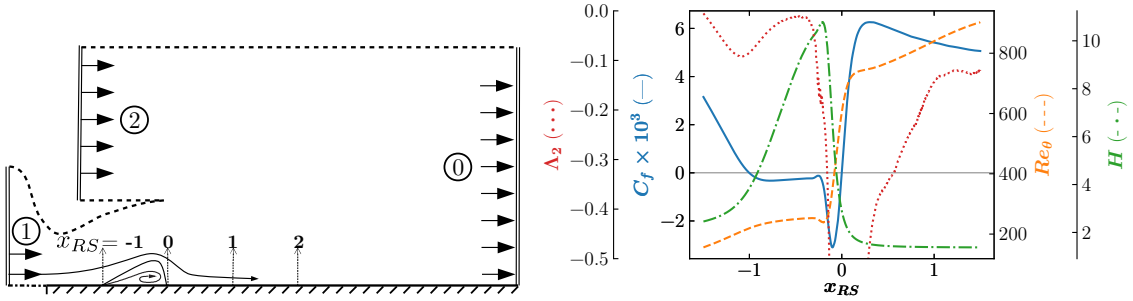

Fig. 1 Flow configuration (DNS by Laurent *et al.* [48]) used as reference for calibration purposes, with exaggerated wall-normal scaling, and main boundary-layer parameters.

leading-edge region of a OA209 airfoil near stall (Richez et al. [2, 50]). The freestream Mach number and chord-based Reynolds number of this airfoil configuration are, respectively: $M_\infty = 0.16$ and $Re_c = 1.8 \times 10^6$. The flow coming from ① and ② is laminar, and separates from the no-slip wall as a consequence of the adverse pressure gradient. Downstream of the laminar separation, the flow transitions to turbulence and reattaches to the no-slip wall, forming the transitional bubble sketched in Fig. 1. Downstream of the bubble, the streamwise pressure gradient becomes zero, as the curved upper slip wall terminates tangentially to the flow direction.

The DNS results of Laurent et al. [47, 48] are used in this study. The dimensionless boundary-layer parameters (Fig. 1) are

$$\Lambda_2 = \frac{\theta^2}{\nu}\frac{dU_e}{dx} \quad ; \quad c_f = \frac{2\mu\partial_y u|_0}{\rho_e U_e^2} \quad ; \quad Re_\theta = \frac{\rho_e U_e \theta}{\mu_e} \quad ; \quad H = \frac{\delta^*}{\theta} \quad ; \quad x_{RS} := \frac{x - x^R}{x^R - x^S} \tag{2}$$

where Λ_2 is the Pohlhausen parameter (which reaches a minimal value of -3.5 in the neighborhood of the reattachment point), c_f is the skin-friction coefficient, Re_θ is the momentum-thickness Reynolds number, H is the boundary-layer shape factor, and x_{RS} the streamwise coordinate scaled by the length of the bubble (x^R and x^S are the reattachment and separation points of the DNS calculations). Several flow regions are identified by the time-averaged DNS results

- $x_{RS} < -1$, Attached laminar flow
- $-1 \leq x_{RS} < 0$, Short transitional bubble where $c_f < 0$. This region can be subdivided in two parts, the separated laminar boundary-layer ($-1 \leq x_{RS} < x_{RS}^{tr} = -0.27$) followed by the separated transitional region ($x_{RS}^{tr} = -0.27 \leq x_{RS} < 0$) characterized by a high rate of

production of turbulence and sudden increase in Re_θ (at $x_{RS}^{tr} = -0.27$).

- $0 \leq x_{RS} < 2$, Relaxation boundary-layer: The attached boundary-layer downstream of the bubble is not yet fully turbulent, since the log-law is not completely established. Specifically, the velocity profile predicted by the DNS lies below the theoretical log-law [51, 52]. In this region there is a local positive peak of skin-friction coefficient and a pronounced boundary-layer thickness growth rate.

- $2 \leq x_{RS}$, Fully-developed turbulent boundary-layer: The attached turbulent boundary-layer is well established and the log-law is verified. The streamwise pressure gradient is null. In this region, as shown by Laurent et al. [48], the budget of the turbulent kinetic energy is in close agreement with the DNS results obtained by Spalart [53] for an attached turbulent boundary layer.

B. Results with existing models

Laurent *et al.* [48] compared k-ω results with fixed transition location and an arbitrarily prescribed streamwise-variable intermittency-function with the DNS data. In Fig. 2 we present the predictions of the reference flow with the Langtry-Menter γ-$\overline{Re_\theta}$ model [54, 55], and with the Wilcox 2006 k-ω [56], both with ($C_{\rm lim} = 1$) and without shear limiter ($C_{\rm lim} = 0$). For the Wilcox 2006 model, the production terms of the turbulence equations were disabled in the laminar region upstream of transition onset where they were instantly activated. This kind of activation is hereafter referred to as *Step*. The transition onset was prescribed at the DNS-computed location ($x_{RS}^{tr} = -0.27$).

It can be observed from Fig. 2 that no model properly predicts the DNS flow topology. The boundary-layer quantities are expressed as a function of the dimensionless coordinate x_{RS}, Eqn. (2). The Langtry-Menter model predicts correctly the location of transition, as the coordinate from which Re_θ grows abruptly is fairly close to the DNS data. However, the bubble length is overestimated by about 30%, and both c_f and Re_θ are overestimated downstream of the bubble.

The Step-activated model are sensitive to the use of a shear stress limiter, as observed in Fig. 2. Surprisingly, if no shear limiter is employed, the bubble length is correctly predicted, as the reattachment point is overestimated by just 6% of the bubble length. However, if the shear limiter

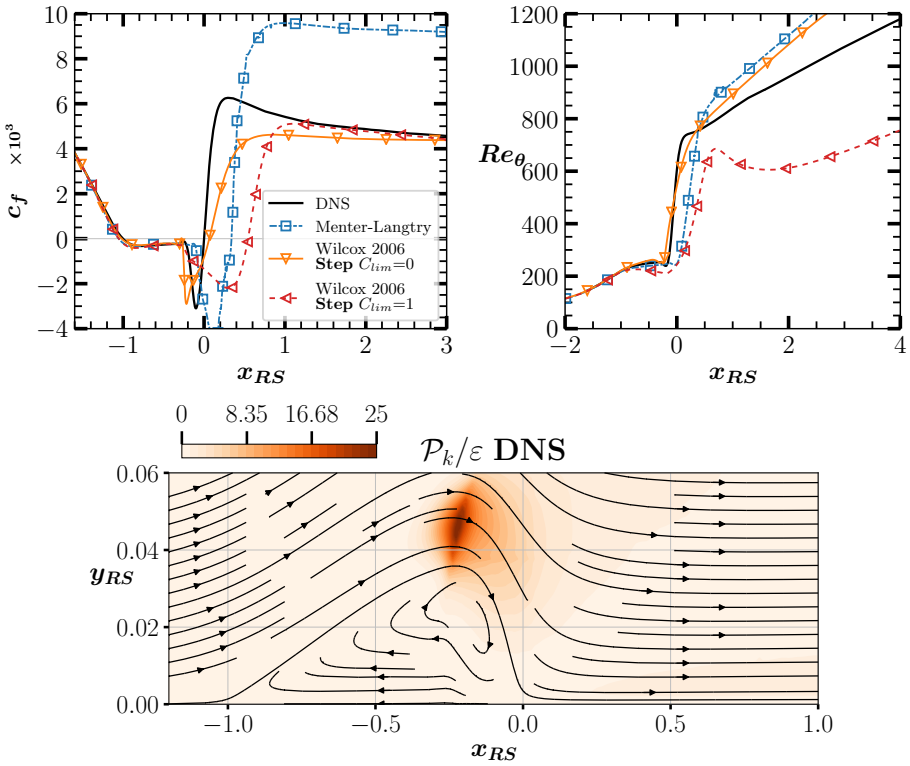

Fig. 2 Classical activations of turbulence models applied to the prediction of the reference flow of Laurent *et al.* Production-to-dissipation ratio calculated from the DNS data (in the laminar region, $\varepsilon^{(\tau)}$ was clipped by its value at the transition onset)

is activated, a significant overestimation of the bubble length of 55% is produced. The Re_θ plot effectively shows that the use of the shear limiter massively reduces the rate at which Re_θ increases downstream of the bubble. The reason of this noticeable impact of the shear limiter is related to the production of the Reynolds stresses. Indeed, the shear limiter indirectly reduces the rate of growth of the production of k, which translates into an underestimation of the Reynolds shear-stress, as will be shown in the following sections. As a result, the diffusion of momentum is comparatively lower, which delays reattachment.

Withal, an important observation is related to the production-to-dissipation of turbulence of the reference flow $\mathcal{P}_k/\varepsilon^{(\tau)}$, where

$$\mathcal{P}_k = -\overline{\rho u_i' u_k'}(\partial_k \overline{u_i}) \quad ; \quad \rho\epsilon^{(\tau)} = \overline{\tau_{ik}' \frac{\partial u_i'}{\partial x_k}} \tag{3}$$

This ratio (Fig. 2) is representative of the departure of turbulence from equilibrium. We remark that $\mathcal{P}_k/\varepsilon \gg 1$ in the shear layer of the transitional region, which indicates a fast growth of the

turbulence provoked by the rapid breakdown to the turbulence. Current k-ω turbulence models experience difficulties in properly modeling the effects of this pronounced non-equilibrium region, and as a result, the bubble topology is poorly predicted and therefore the predicted downstream development of the turbulent boundary layer may yield unrealistic results, as shown in Fig. 2. In turn, if the bubble topology was better predicted by improving the capacity of the turbulence models to account for the aforementioned non-equilibrium region effects, then the history effects related to the bubble would be correctly modeled, and the turbulent boundary layer predictions downstream of the bubble would be more realistic.

Several authors have made similar observations and have come to the conclusion that the effects of the non-equilibrium region could be modeled by boosting the production term of the turbulence model. Arnal [49] was one of the first authors to suggest a 'boost' of the production of the turbulence in the transitional region of the laminar separation bubble by means of a non-local transition function, not necessarily linked to the physical intermittency factor. Langtry & Menter [18] γ-$\overline{Re_\theta}$ model proposed a fully-local boost mechanism of the production term of k by means of an "effective" intermittency that can yield values higher than one: $\widetilde{\mathcal{P}_k} = \gamma_{\text{eff}}\mathcal{P}_k$. Recently, Menter et al. [22] proposed a new local approach of boosting the $\mathcal{P}_k$ term that accounts for both attached and separation-induced transition. These authors effectively observed that the original SST model required an overlong length to build-up turbulence in the boundary layer. Their production term of k includes a new contribution, which is also dependent on the intermittency factor. Kubacki and Dick [29] also proposed a local boosting of the production term of k in order to model the separation-induced transition. The boosting strategy proposed by Kubacki and Dick is similar to the Menter et al. [22] approach, in the sense that a new supplementary contribution is added to the original production term.

In summary, fundamentally two conclusions based on the previous observations constitute the foundations of the proposed model that is presented in the next section, namely: (a) boosting the production of turbulence seems appropriate to account for the non-equilibrium effects of the transitional region, and (b) the use of the shear limiter will be avoided in the transitional region in order to allow for sufficiently fast growth of the turbulence.

III. LSTT model formulation

In this section we present the proposed model, denoted 'LSTT' for Laminar Separation Transition Triggering. In contrast to the 'Step' approach, where the source terms of the turbulence model are set to zero in the laminar regions and instantly activated from the transition onset location, the new model introduces streamwise-variable weighting of turbulent production.

A. Correlations for transition onset location

The location of the transition onset is calculated by the empirical correlation of Roberts [43], and by the combined criteria of Arnal et al. [44] and Gleyzes [45], following equation (4)

$$s_{tr} = \min(s_{\text{Roberts}}, s_{\text{AHD-Gleyzes}}) \tag{4}$$

Details on the correlations, which provide s_{tr} with input the calculated boundary-layer parameters ($Re_\theta(s)$, $H(s)$, Λ_2) and the turbulence intensity $T_u(s)$ at the boundary-layer edge, are given in the appendix.

B. Transition triggering in k-ω

In the present work we model the smooth rise of turbulence from transition onset, s_{tr}, to the point where the fully turbulent k-ω model is applied, s_c, by introducing two modifications to the k-ω equations (written below in a generic form, which can represent different model variants).

$$\partial_t(\rho k) + \partial_i(\rho\overline{u_i}k) = f^{tr}(-\rho\overline{u_i'u_j'})(\partial_j\overline{u_i}) - \beta_k\rho\omega k + \partial_i[(\mu+\sigma_k\mu_t)\partial_i k] \tag{5a}$$

$$\begin{aligned}\partial_t(\rho\omega) + \partial_i(\rho\overline{u_i}\omega) =& \min(f^{tr},1)\alpha_\omega\frac{\omega}{k}(-\rho\overline{u_i'u_j'})(\partial_j\overline{u_i}) - \beta_\omega\rho\omega^2 + \partial_i[(\mu+\sigma_\omega\mu_t)\partial_i\omega] \\ &+\sigma_d\frac{\rho}{\omega}\max((\partial_i k)(\partial_i\omega),0)\end{aligned} \tag{5b}$$

$$(-\rho\overline{u_i'u_j'}) \approx 2\mu_t\overline{S_{ij}} - \frac{2}{3}\rho k\delta_{ij} \tag{5c}$$

$$\mu_t = \frac{\rho k}{\max\left\{\omega; C_{\text{lim}}\sqrt{\frac{2\lambda_1\overline{S_{ij}}\,\overline{S_{ij}}+2\lambda_2 F_2^2\overline{\Omega_{ij}}\,\overline{\Omega_{ij}}}{(\lambda_1+\lambda_2)\beta_k}}\right\}} \tag{5d}$$

- The non-negative dimensionless transition function $f^{tr}(s)$, weights the production term of the

k equation. It was designed to trigger the transition at the location of the transition onset s_{tr} (Eq. (4)) . It is not an intermittency function as it is not bounded by 1.

- The production term of the ω equation is weighted by $\min(f^{tr}, 1)$. The authors found that limiting the value of the weighting factor of the production of ω was necessary in order to avoid an undesired boosting of the destruction of k when $f^{tr} > 1$. This is required in order to allow a rapid enough growth of the net production of turbulence in the transitional region.

- Preliminary tests showed that the shear stress limiter reduced turbulence production in the bubble shear layer where transition occurs. It is therefore enabled once the boundary-layer reaches a fully turbulent state. This is accomplished via the C_{lim} coefficient.

The shear stress is limited using the blending function F_2 proposed by Menter [35]. We have used the same nomenclature as Wilcox [41] regarding the coefficient C_{lim}. In the original Wilcox 2006 k-ω model, $\lambda_1 = 1$, $\lambda_2 = 0$ and $C_{\text{lim}} = 7/8$. A value of $C_{\text{lim}} = 0$ would disable the stress limiter. However, for this study we employ $\lambda_1 = 0$ and $\lambda_2 = 1$, similarly to the Menter SST formulation.

Although a compressible flow solver was used [57], given the low Mach numbers of the cases studied, we use an incompressible formalism for the presentation of the model. All equations can be readily extended to a compressible framework, invoking Morkovin's hypothesis [58] and replacing S_{ij} by its deviatoric part $S^d_{ij} = S_{ij} - \frac{1}{3} S_{mm} \delta_{ij}$.

C. Triggering functions

In the present work, we propose C_{lim} to be a zonal 1D function along the transition lines, similarly to the transition function f^{tr}. Therefore, both f^{tr} and C_{lim} are functions of the transition line dimensionless streamwise coordinate, $\widehat{s}$, defined by Eqn. (1).

By construction, $\hat{s} = -1$ at the laminar separation point and $\hat{s} = 0$ at the transition onset.

We propose a transition function $f^{tr}(\hat{s})$ adapted to each considered k-ω model. The functions are built using simple piecewise Hermite polynomials with continuous tangents (C^1 continuity). The general form of $f^{tr}(\hat{s})$ is

$$f^{tr}(\hat{s}) = \begin{cases} 0 & (\hat{s} < 0) \\ a\left(-2\left(\frac{\hat{s}}{\widehat{s_a}}\right)^3 + 3\left(\frac{\hat{s}}{\widehat{s_a}}\right)^2\right) & (0 \le \hat{s} < \widehat{s_a}) \\ 2\left(\frac{\hat{s}-\widehat{s_a}}{\widehat{s_b}-\widehat{s_a}}\right)^3 (a-1) - 3\left(\frac{\hat{s}-\widehat{s_a}}{\widehat{s_b}-\widehat{s_a}}\right)^2 (a-1) + a & (\widehat{s_a} \le \hat{s} < \widehat{s_b}) \\ 1 & (\hat{s} \ge \widehat{s_b}) \end{cases} \tag{6}$$

The stress limiter is controlled by means of the coefficient $C_{\lim}(\hat{s})$ as shown in equation (7). Specifically, the stress limiter is disabled in the bubble and in the neighborhood of the reattachment point, and enabled several bubble lengths downstream of the reattachment point. As anticipated in section II B, disabling the stress limiter in the bubble is necessary in order to allow the models to reach high values of production-to-dissipation ratio sufficiently fast, as it has been observed in DNS simulations.

$$C_{\lim}(\hat{s}) = \begin{cases} 0 & (\hat{s} < \widehat{s_c}) \\ 1 & (\hat{s} \ge \widehat{s_c}) \end{cases} \tag{7}$$

The functions $f^{tr}(\widehat{s})$ and $C_{\lim}(\widehat{s})$ vary as eqns. (7) and (6) along the transition lines [46], but they are indeed applied throughout the entire flowfield by means of simple orthogonal extrusion from the wall. The transitional extensions presented in this study have been intentionally designed to be simple, as we only act on the production terms of the turbulence equations and on the stress limiter by means of 1D transition functions. In order to apply the transitional model, one needs to compute the laminar separation point s_{sep} along the transition line; predict the transition onset s_{tr} by means of transition criteria; and finally apply the appropriate closure constants for $\widehat{s_a}$, $\widehat{s_b}$, $\widehat{s_c}$ and a.

In the following section we present the proposed calibration of the set of constants $\widehat{s_a}$, $\widehat{s_b}$, $\widehat{s_c}$, and a, adapted to each of the four different k-ω models considered in this study. The calibration has been performed based upon the DNS data of the reference flow presented in section II. We initially apply the model to the Wilcox 2006 k-ω model [56], and we then extend it to the Wilcox 1988 [59], Kok [60] and Menter SST [61] models.

IV. Calibration

A. Numerical method and boundary conditions

The simulations were run using the Navier-Stokes solver elsA [57] developed at ONERA and post-processed using the code Cassiopee [62] developed at ONERA. The post-processing functions are employed in exactly the same fashion to the available time-averaged DNS fields and the RANS simulations results.

The computations were run on a 2D mesh of 560946 nodes distributed in 14 structured blocks. The height of wall adjacent cells is such that $\Delta y^+ < 1$ everywhere in the turbulent boundary-layer, and there are about 250 streamwise points in the reversed-flow region belonging to the separation bubble. A grid-convergence study will be presented in paragraph IV D.

A typical problem of two-equation models at the farfield is the specification of appropriate values ensuring both sufficiently slow decay and low values of μ_t. Rumsey [63] notes that the numerical transition to turbulence may depend on the free-stream values of the turbulence variables. It may also depend on their cut-off values. The free-stream and numerical cut-off values employed in this study are

$$(\rho k)_\infty = \frac{3}{2} T_{u\infty}^2 V_r^2 \rho_r \qquad (\rho\omega)_\infty = \frac{\rho_r (\rho k)_\infty}{0.01 \mu_\infty} \tag{8}$$

$$(\rho k)_{\text{cut-off}} = 10^{-2} (\rho k)_\infty \qquad (\rho\omega)_{\text{cut-off}} = 10^{-2} (\rho\omega)_\infty \qquad (\mu_t)_{\text{cut-off}} = 10^{-3} \mu \tag{9}$$

The reference values employed are: $T_{u\infty} = 0.01 \times 10^{-2}$; $\rho_r = 1.21$ kg·m^{-3}; $V_r = 55$ m·s^{-1}, where the subscript r stands for reference. These settings verify the recommendations of Rumsey and Spalart [64].

The wall condition on ω is implemented assuming values at the centers of wall-adjacent cells equal to $\omega = 6\nu/\beta y^2$. The inflow and boundary conditions on the γ-$\overline{Re_\theta}$ quantities, for the Langtry-Menter [18, 54] model, are set as follows

$$\gamma_\infty = 1, \qquad \overline{Re_\theta}_\infty = 1173.51 - 589.428 T_{u\infty} + 0.2196 / T_{u\infty}^2 \tag{10}$$

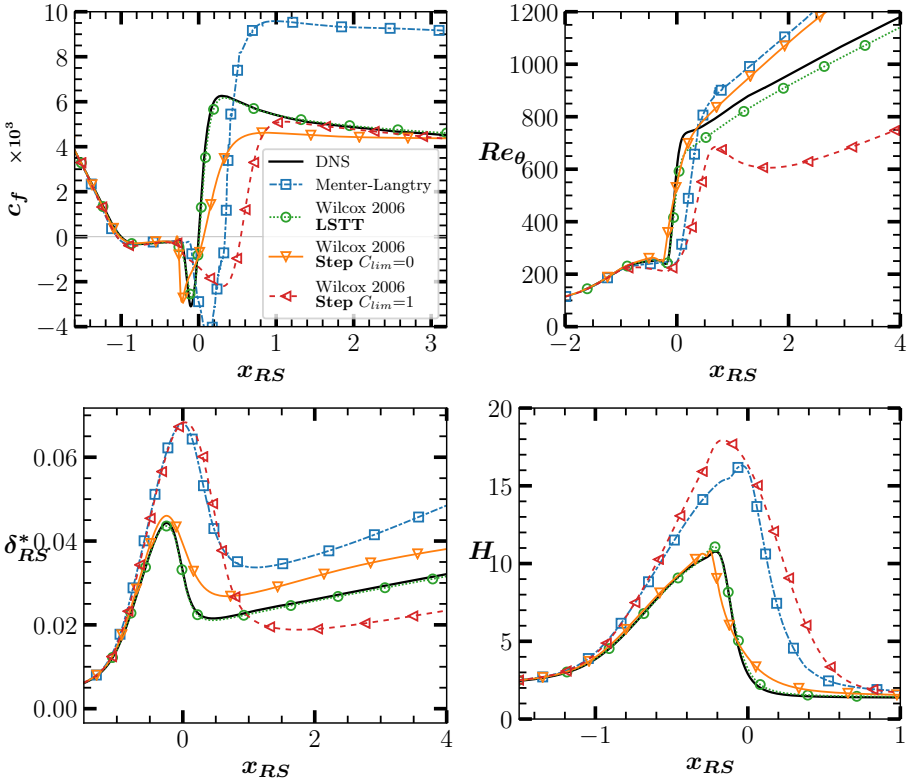

Fig. 3 Comparison of the LSTT model with existing approaches for the prediction of velocity profiles, both in linear (above) and in log-scale (below) for the reference flow of Laurent *et al* [48].

The transition onset location is accurately predicted by the Roberts criterion at $x^{tr}_{RS} = -0.27$ for a turbulence level of $T_u = 0.1 \times 10^{-2}$. One may note that, as shown in the Appendix, the Roberts criterion is insensitive to turbulence levels lower than $T_u < 0.1 \times 10^{-2}$.

B. Closure coefficients applied to Wilcox 2006

The calibration of the closure constants (shown in table 2) aimed at satisfying mainly two constraints. The first constraint consists in the bubble reattachment point being close to the DNS reattachment point. The second constraint consists in the local maximum peak of skin-friction being close to the DNS value. The results (Fig. 3 and 4) indicate that these constraints are adequate to obtain satisfactory agreement with the DNS mean bubble dimensions. The skin-friction coefficient is defined as $c_f = \tau_w / 0.5 \rho_e U_e^2$ and the dimensionless boundary-layer displacement thickness scaled by the DNS average bubble size is expressed $\delta^*_{RS} = \delta^* / (x^R - x^S)$.

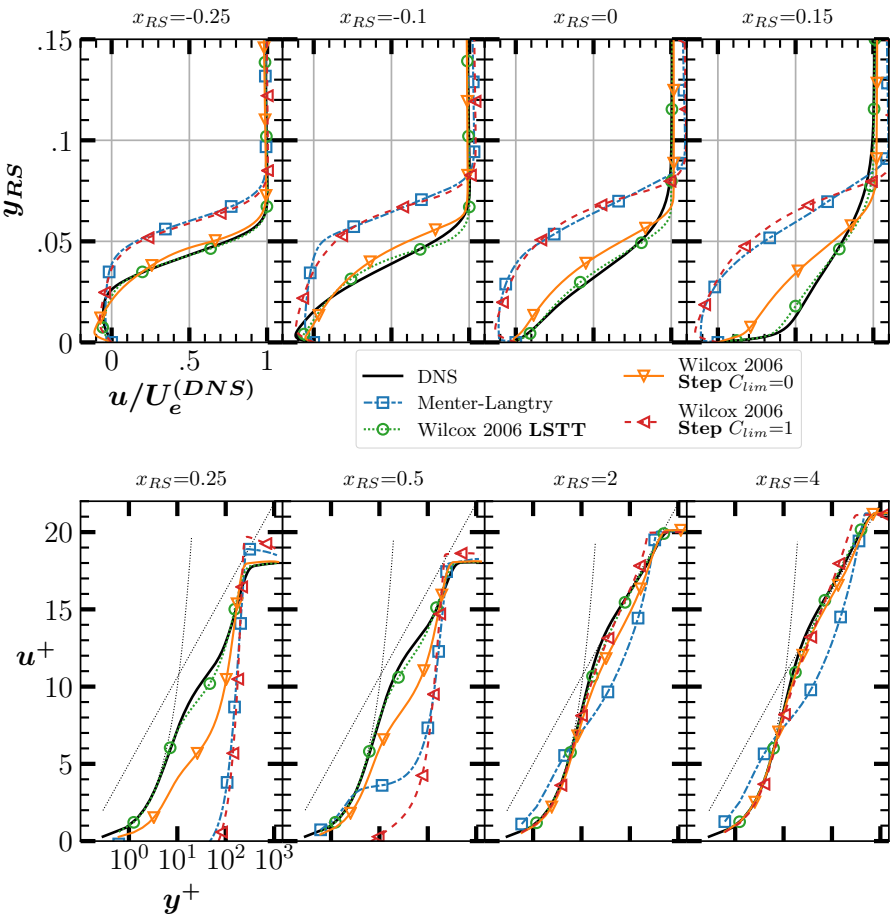

Fig. 4 Comparison of the LSTT model with existing approaches for the prediction of velocity profiles, both in linear (above) and in logscale (below) for the reference flow of Laurent *et al* [48].

As shown in Fig. 2, the Langtry-Menter model and simple 'Step' activation of Wilcox 2006 yield a bubble which is longer than DNS. As a result, in Fig. 3 we can observe that the shape factor of these two models reach very high maximum values. There is an important history impact of the bubble upon the downstream turbulent boundary-layer predictions. The Langtry-Menter model overestimates the thickening rate of the boundary-layer, as observed through the values of δ^*_{RS} and Re_θ downstream of $x_{RS} = 1$. We can observe that the LSTT model properly reproduces the separation and reattachment points and positive peak of skin-friction coefficient, thus corroborating that the calibration constraints have been respected. Furthermore, the LSTT model also predicts closer values for the other boundary-layer quantities (Re_θ, H and δ^*_{RS}) with respect to the DNS data.

Several velocity profiles are shown in Fig. 4, where the theoretical inner viscous layer $u^+ = y^+$ and the log-law layer $u^+ = \frac{1}{0.41} \ln y^+ + 5$ laws are also shown (thin dotted curves). It can be observed that the log-law is not fully established by the DNS mean field upstream of $x_{RS} = 2$. We remark that among the different compared models, only the Wilcox 2006 LSTT model correctly predicts the velocity profiles, both in the separated and in the reattached region. The log profiles indicate that models using a shear limiter predict an overlong transitional region until fully turbulent conditions are reached. The same observation applies to a lesser extent to the Wilcox 2006 model without shear limiter and Step activation. The LSTT model correctly transitions at the same rate as the DNS data, indicating again that the history effects related to the bubble have been properly modeled. Inside the LSB ($x_{RS} \leq 0$), we can see that the deficit of velocity is overestimated by both the Menter-Langtry model and the Step activation. This confirms the overestimation of the slope of δ^*_{RS} observed previously in Fig. 3. Disabling the shear stress limiter ($C_{\text{lim}} = 0$) slightly reduces the differences with DNS, as it allows a comparatively faster turbulence growth, thus reducing the separation extent.

Indeed, in Fig. 5 we can observe the significant effect of the LSTT with respect to a simple activation with no shear limiter delay. Plots (a) and (b) show a good qualitative agreement of the Reynolds shear stress. In the other hand, plot (c) and (d) show poor agreement of the Reynolds shear stress compared to the DNS data. This lack of production of $-\overline{u'v'}$ observed in (c) and (d) is mainly due to two reasons: (1) the shear limiter has an opposing effect to the large production rate of Reynolds stress in the transitional region; and (2) from the transition onset, a simple "*off/on*" step activation of the source terms of the model does not suffice to properly account for the rapid turbulence growth rate of the transitional region. The LSTT approach introduced in section III addresses both these issues.

C. Calibration for other k-ω variants

The LSTT approach (6)-(7) can be adapted to other k-ω variants, as the Wilcox 1988, Kok and Menter SST. Since each k-ω version naturally yields different boundary-layer development behavior [65], a specific calibration of the LSTT closure coefficients adapted to each variant is required. The

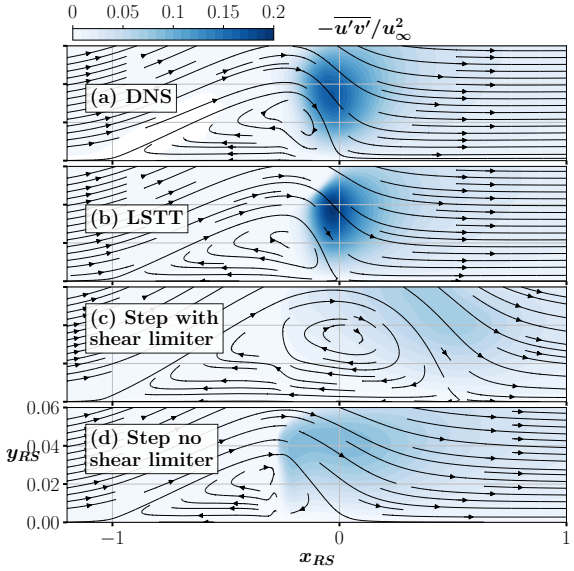

Fig. 5 Shear Reynolds stress, $-\overline{u'v'}$, scaled by the free-stream reference velocity u_∞, for: (a) the DNS data from [48]; (b) The Wilcox 2006 LSTT transitional extension proposed in this study; (c) Simple step activation of the Wilcox 2006 model, with the stress limiter activated everywhere ($C_{\text{lim}} = 1$); and (d) Simple step activation of the Wilcox 2006 model, with the stress limiter disabled ($C_{\text{lim}} = 0$). The subscript $(\bullet)_{RS}$ means that the coordinate has been scaled with respect to the DNS-computed bubble length.

	$\widehat{s_a}$	$\widehat{s_b}$	$\widehat{s_c}$	a
Wilcox 2006	0.182	0.414	5.83	2.15
Kok	0.200	0.620	5.83	2.23
Menter SST	0.312	0.544	5.83	2.20
Wilcox 1988	0.086	0.487	3.78	1.85

Table 2 Models coefficients for the LSTT model

closure coefficients are presented in table 2, and the resulting $f^{tr}(\widehat{s})$ functions and skin-friction predictions are shown in Fig. 6.

The proposed calibration shows acceptable agreement between the RANS models and the DNS data. All models yield the laminar separation at the same location ($x_{RS} = -1$), which coincides with the location of the laminar separation of the DNS results. The reattachment point is also located at the same point ($x_{RS} = 0$) for all the models and the DNS, which shows that the main design requirement has been satisfied. All models produce a local minimum peak of skin-friction

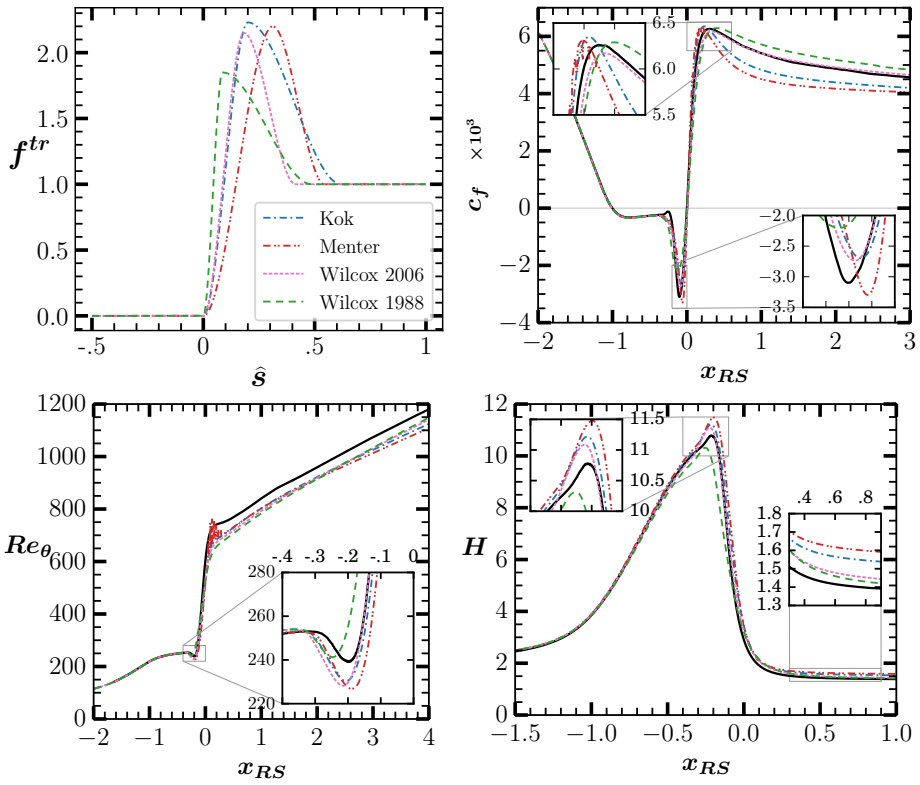

Fig. 6 Transition function and global boundary-layer parameters predicted by the LSTT models for the four k-ω variants. DNS data is marked ——.

just upstream of the reattachment point. The maximum skin-friction peak right downstream of the reattachment point is also fairly well predicted by all the models. The most significant deviations from the DNS results are observed further downstream (from $x_{RS} > 0.5$). In this region, we can clearly observe that the Kok and Menter models tend to under-predict the skin-friction values, whereas the Wilcox 1988 model slightly overpredicts it. The relative differences on the c_f values downstream of the bubble were discussed by Bernardos *et al.* [65]. In short, the classification by decreasing order of diffusivity of the turbulent boundary layer for the models is: Wilcox 1988, Wilcox 2006, Kok and finally Menter. As the diffusivity, or similarly, the growth rate of the turbulent boundary layer, is related to the prediction of the skin-friction via the Von-Kármán integral equation, we find the same trend in the skin-friction predictions. In summary, the calibration of all models respect to the DNS data is acceptable, which justifies the choice of the formulation of the LSTT approach for predicting this kind of flow.

GRID	$N_i^\dagger$	$N_j^\dagger$	$\Delta y^+_{(x_{RS}=2)}$	$N_{\delta(x_{RS}=2)}$
r2	1428	330	0.29	254
ry2	714	330	0.29	254
Baseline	714	165	0.58	127
c2	357	165	0.58	127
c4	178	165	0.58	127
c8	89	165	0.58	127

Table 3 Considered meshes for grid-assessment. †: the number of points concerns the region $-1 \leq x_{RS} \leq 2$ and $0 \leq y_{RS} \leq 0.5$. The last column indicates the approximate number of points in the boundary layer.

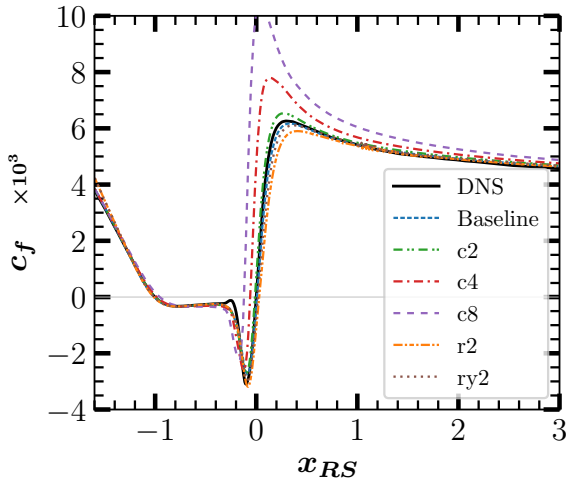

Fig. 7 Skin-friction for the grids considered in table 3 and the Wilcox 2006 LSTT model.

D. Grid convergence study

We examine the grid-dependency of the Wilcox 2006 LSTT model proposed in the previous section. Six grids are considered, as shown in table 3. The grid labeled *Baseline* is the mesh that has been used in sections IV A to IV C. It is the same grid employed by Laurent et al. [47] to assess the Wilcox 1988 turbulence model for the reference configuration [48].

The skin-friction and velocity profiles are shown in figures 7 and 8. It can be observed that reasonable convergence is reached for the grid labeled *c2*, which is twice coarser than the *baseline* grid in the streamwise direction. The grid labeled *ry2* is twice finer than *baseline* in the wall-normal direction, and no significant difference is observed with respect to the *baseline*. The finest grid,

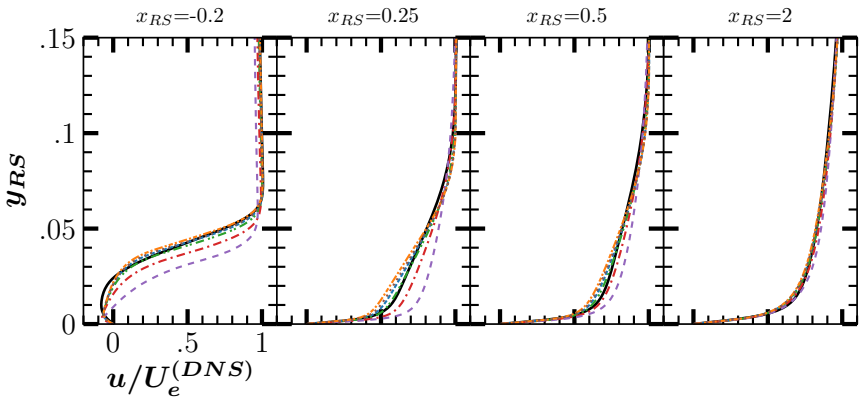

Fig. 8 Velocity profiles mesh convergence for the grids considered in table 3 and the Wilcox 2006 transitional extension proposal. Legend: *r2* grid -·-·-; *ry2* grid ·····; *Baseline* grid ---; *c2* grid - - -; *c4* grid -·-·-; *c8* grid - - -; and DNS data ——.

labeled *r2*, which is twice finer in both directions than *baseline*, yields comparable results with respect to the *baseline* grid, with only a slightly less pronounced c_f positive peak, which can be observed at $x_{RS} \approx 0.25$.

As observed in Fig. 7, there is a clear trend in the results when the streamwise discretization is coarsened. As the mesh is coarsened streamwise, the bubble size is reduced, the positive peak of skin-friction becomes more pronounced, and the negative peak is reduced. Remarkably, downstream of the bubble, for $x_{RS} \gtrapprox 2$, the differences between the grids are mitigated, as the c_f and velocity profiles shown in Fig. 8 tend to merge. This seems logical, as the streamwise mesh quality is expected to affect more the predictions inside the bubble, but less so the downstream development of the turbulent boundary-layer. Actually, an interesting consequence of this observation is that if too coarse a mesh is employed, say e.g. grid *c8*, the bubble is poorly predicted, but the history effects on the downstream boundary-layer seem to have little impact on the skin-friction and velocity profile predictions, provided that the wall-normal discretization is of acceptable quality.

The results of grids c_2, *Baseline*, r_{y2} and r_2 grids are close. Considering that the streamwise discretization law is nearly homogeneous, the number of streamwise points contained in the bubble is about 1/3 of the N_i points shown in table 3. As a consequence, it appears that streamwise grid convergence is achieved by 120 stations within the bubble. Furthermore, as the downstream

boundary-layer predictions of the grid $c8$ are acceptable in spite of a poor prediction of the bubble itself, we remark that 30 streamwise points inside the bubble are enough for a fair prediction of the downstream turbulent boundary-layer, which is the actual target for many applications.

V. Validation test cases

In the current section we present two different validation test cases: the NACA 0012 airfoil at 10.55° of angle of attack and Re_c=100,000; and the wind-turbine airfoil S809 at 1.01° and Re_c=2×10^6. These test cases have been chosen because they cover a wide range of chord-based Reynolds number (low and high Reynolds number), the airfoils have very different geometries, and also the operating angles of attack are very different. Hence, these two cases are challenging validation flows for the proposed model.

In order to show how the model behaves under application conditions (with no a priori knowledge of the transition onset location), the NACA 0012 airfoil case has been computed by coupling the proposed model to the transition criteria of AHD-Gleyzes and Roberts.

As mentioned in section III, the presented models require the prediction of the transition onset location, noted s_{tr}, in the curvilinear abscissa frame of the transition line (airfoil surface), noted s. In the current application test case, we use simultaneously two transition criteria: the Roberts [43] criterion, and the AHD [44] Gleyzes [45] criterion. Further details of these criteria are found in the original publications, and a brief description is given in the Appendix. A summary of the specific implementation in the elsA code of these criteria was reported by Cliquet *et al.* [46] and Perraud *et al.* [66].

Both Roberts and AHD-Gleyzes criteria are sensitive to a critical external turbulence rate. For the present computations, we applied a characteristic external turbulence rate of 0.1%, which can be considered representative of a low-turbulence atmosphere. Following Mack's relationship [67], this turbulence level translates to a critical total amplification rate of $N_{cr} = 8.15$.

The Roberts criterion, which is completely empirical, is best adapted to short transitional bubbles characteristic of high chord-based Reynolds number airfoils. For low-Reynolds number flows around airfoils, this criterion tends to predict an unrealistically far downstream transition onset.

On the other hand, the AHD-Gleyzes criterion, which has been designed employing more profound physical foundations, is better suited to low-Reynolds number flows than Roberts criterion. However, from the authors' experience, AHD-Gleyzes criterion is very sensitive to the flow topology, and this can result in convergence difficulties, specially in the transient period right after the simulation initialization. This is the reason why we combined these two criteria [Eqn. (4)], Roberts would ease the convergence in the initial iterations, and then a realistic transition onset is obtained by AHD-Gleyzes criterion.

A. NACA0012 test case

The results presented in this paragraph are compared to the LES computations of Alferez et al. [68]. For this case, we compare the results of the LSTT model applied to the Wilcox 2006 k-ω with the predictions of Langtry-Menter γ-$\overline{Re_\theta}$ model and the criteria-based approach with simple Step activation.

The mesh is of C-type, and it has been generated through wall-normal hyperbolic extrusion using Cassiopee [62]. At least 60 normal points are contained in the boundary-layer. The wall-adjacent cell height is such that $\Delta y^+ < 1$ everywhere along the airfoil where the boundary-layer is turbulent. About 150 streamwise points are present between $0.001 < x/c < 0.1$ in the suction side, which is the region where the transitional bubble should appear following the LES data.

In Fig. 9 the airfoil skin-friction coefficient is calculated as $c_f = \tau_w/(0.5\rho_\infty U_\infty^2)$ and the pressure coefficient as $C_p = (p - p_\infty)/(0.5\rho_\infty U_\infty^2)$.

We can observe in Fig. 9 that the best overall agreement is achieved with the LSTT model. The Langtry-Menter model predicts correctly the location of the transition onset, at about $x/c = 0.07$, but fails to predict the reattachment and, as a consequence, the formation of the bubble. The evolution of the boundary-layer parameters Re_θ and H is also strongly affected by the models. The failure to reattach shortly downstream of the transition onset for the Step activation with shear limiter and the Langtry-Menter models provokes too pronounced a thickening of the boundary-layer, due to the massive detached flow characteristic of the stalled condition. On the other hand, the Wilcox 2006 LSTT model shows a reasonably accurate growth of Re_θ, closely following the LES

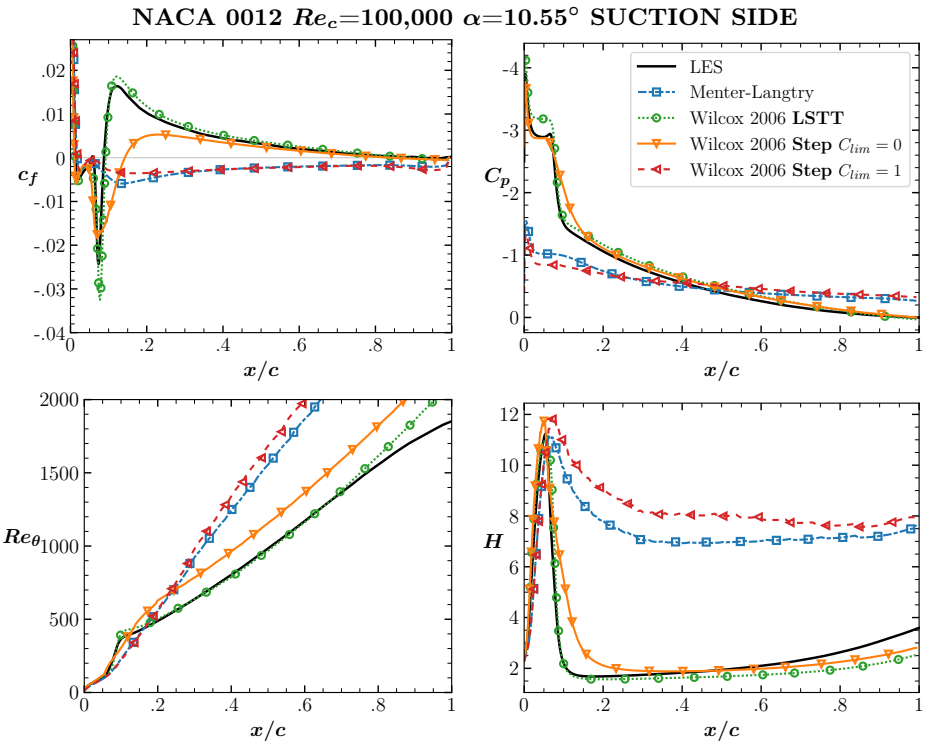

Fig. 9 Boundary-layer parameters on the suction side of the NACA 0012 airfoil predicted by several models and compared with LES results [68].

data. A simple Step activation without stress limiter ($C_{\text{lim}} = 0$) predicts a bubble (reattachment) but with a 60% overestimation of its length. Interestingly, the step-activation without shear limiter correctly predicts the C_p distribution up to the end of the bubble plateau (the transition onset), whereas the proposed activation of the Wilcox 2006 overestimates the C_p values of the plateau. The reasons of this behavior are unknown to the authors, and it has been observed also for the Wilcox 1988 model predictions, but not for the Kok and Menter SST turbulence models when the proposed LSTT is performed (not shown).

The resulting velocity profiles can be observed in Fig. 10. The Wilcox 2006 LSTT turbulence model produces an important improvement with respect to the other considered methodologies near the bubble region. Far downstream of the bubble, from $x/c > 0.5$, the agreement of the LSTT model with the LES data is acceptable, but surprisingly the simple Step activation is fairly close to the data as well. This could be anticipated by observation of the H evolution in Fig. 9. Indeed, from about $x/c > 0.3$ the evolution of H for the Step activation without stress limiter is closer

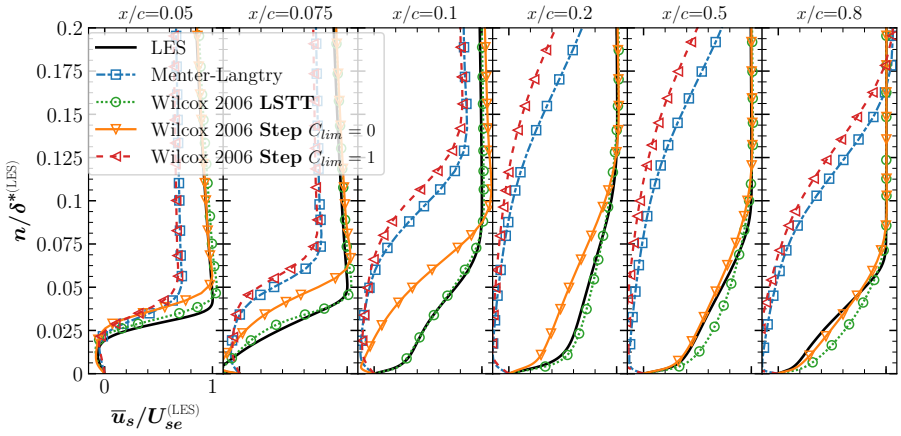

Fig. 10 Comparison of velocity profiles for several models for the NACA 0012 test case [68]. The airfoil-tangential velocity $\overline{u}_s$ is plotted against the airfoil's wall-normal direction n. The tangential velocity component has been scaled by its value at the boundary layer edge of the LES data $U_{se}^{(\mathbf{LES})}$. The airfoil's distance to the wall n has been scaled with respect to the integral displacement thickness of the LES data $\delta^{*(\mathbf{LES})}$

to the data than the LSTT model. Clearly, this does not mean that the Step activation better models the bubble history effects. Indeed, the LSTT model at, e.g. $x/c = 0.3$, yields much better predictions than the Step activation. Hence, if the history effects are correctly modeled up to the point $x/c = 0.3$, any subsequent deviation from the data is rather related to the turbulence model behavior than the activation model.

B. Wind turbine airfoil test case

In the second test case we apply the LSTT model to the simulation of the flow around the S809 airfoil. Experimental data were published by Somers [5]. This airfoil was designed at the National Renewable Energy Laboratory, and has been tested in the low-turbulence wind tunnel of the Delft University of Technology Low Speed Laboratory. We selected the case Re_c=2×10^6 at an angle of attack of α=1.01°, where two short transitional bubbles appear, one on each side of the airfoil. The C_p distributions are shown in Fig. 11. From AHD-Gleyzes transition criteria and LSTT modeling, the obtained transition onset is located at x/c=0.552 for the top side, and x/c=0.503 for the bottom side. These points approximately correspond to the end of the plateau of C_p shown in the zoomed axis of the Fig. 11, where the C_p shows a rapid recovery towards the "fully-turbulent" distribution

downstream of the bubble. The Step computation transition onset has been explicitly prescribed at the aforementioned locations, in order to assess the impact of the activation of the turbulence model.

The RANS simulations have been performed using the same numerical parameters as the NACA 0012 case presented in §V A. The mesh is such that $\Delta y^+ < 1$ everywhere in the turbulent boundary layer, and the bubbles are discretized with at least 60 streamwise points.

In Fig. 11 we also show a "fully-turbulent" computation employing the Wilcox 2006 model, plotted in dotted lines. The overall agreement with the experimental C_p distribution is quite good. This seems logical, as the chord-based Reynolds number is relatively high. As expected, the fully-turbulent computation fails to reproduce the short transitional bubbles. The dash-dotted curve shows a Step activation of the model, with no delay of the stress limiter ($C_{\text{lim}} = 1$). We can observe that in this case bubbles do indeed appear, but their size is overestimated because the C_p recovery does not occur rapidly enough, as the slope of the C_p curve in the recovery region is not sufficiently steep. This effect is due to a slow turbulence growth in the transitional region, already discussed in the previous paragraphs. Moreover, we observe an overestimation of the C_p values right downstream of the bubble. In solid line we present the LSTT model proposed in this work. The C_p recovery is much faster and in closer agreement with the experiment, which translates into a good estimation of the bubble size. Downstream of the bubble, the C_p is closer to the experiment than the Step activation, but there is still a slight overestimation. Overall, the improvement of the proposed model is satisfactory.

VI. Conclusion

The k-ω models transitional adaptations to laminar separation bubbles show promising results compared to other transition triggering mechanisms where the effect of the bubble is not modeled. During this work, we showed that the accuracy of the predictions depends not only upon the calculation of *where* the transition onset is located, but also on *how* the turbulence models are activated. One of the key features that produced good results is the method of disabling the shear limiter in the transitional region, where the turbulence production-to-dissipation ratio is considerably high.

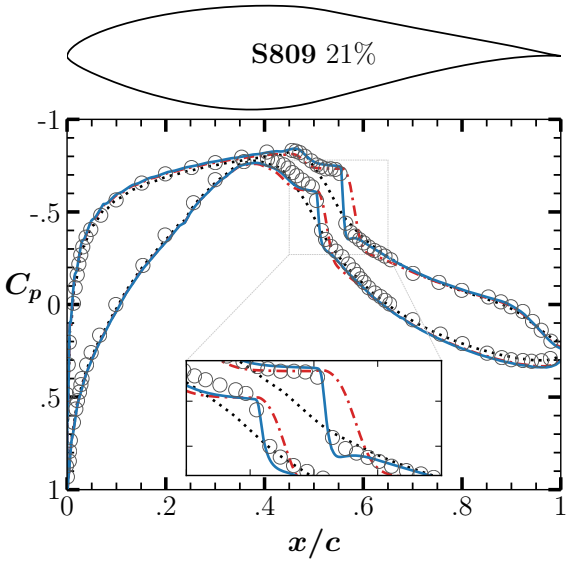

Fig. 11 Pressure distributions on the S809 airfoil at Re_c=2×10^6 and α=1.01°. Legend: Experiment from Somers [5] ◯; Full-turbulent ·····; Step activation -·-·-; LSTT model ——.

This delay mechanism, together with the boosting of the production of turbulence, translated in appropriate predictions of the Reynolds shear stress in the transitional region.

This Laminar Separation Transition Triggering (LSTT) approach assumes that the characteristic length of the transition process within the LSB is the distance between the laminar separation point and the transition onset. Algebraic triggering functions were developed that weight the production terms in the k-ω equations and activate the stress limiter several characteristic lengths (4 to 6) downstream of the transition onset.

The proposed models are not too intrusive into each model's fully turbulent original formulation, in the sense that the closure coefficients are not modified and the original characteristics and behavior of the models are preserved. An asset of the present models is their ease of implementation into CFD codes where the concept of transition lines [46] is included, as the proposed functions are simply one-dimensional. This also makes it easier to combine with other existing transition criteria for natural, by-pass and crossflow transition [46, 66]. The calibration of the model has been performed following constraints based uniquely on the skin-friction coefficient. We observe that this also results in satisfactory predictions of the velocity profiles and Reynolds shear stress. This suggests that the

simple modeling approach of the LSTT is sufficient to correctly predict the main features of a LSB.

The flow used for the calibration of the model is characteristic of a high Reynolds number bubble, typically known as 'short' type. Good results are obtained for high chord-based Reynolds number transitional bubbles, such as in the S809 airfoil case. Additionally, a low-Reynolds number application test case has been studied. This test case consists in the flow around a NACA 0012 airfoil at chord-based Reynolds number of 100,000 and 10.55 degrees of angle of attack, which is very close to the stall condition. The proposed model produced promising results compared to other methods. Considering that the models have been calibrated for a bubble with physical conditions characteristic of an OA209 airfoil at chord-based Reynolds number of 1.8 million, the NACA 0012 airfoil test case is a challenging scenario for the proposed models.

The present work constitute an effort towards the modeling of the effects produced by transitional bubbles encountered in aeronautical applications. However, the models presented herein have been calibrated using a single reference flow, and their universality and applicability to other flows strongly depends on the computation of the transition onset (e.g. by means of transition criteria). Even if these criteria give adequate results for a large range of bubbles, other parameters may be required to describe adequately relevant characteristics of the bubble, and future progress may be achieved by extending the dependence of the transition functions upon such parameters. Further validation and extensions of the proposed models should be undertaken, especially for different chord-based Reynolds number and external turbulence levels.

Appendix

1. Evaluation of boundary-layer parameters

The transition criteria are based on global boundary-layer parameters which are evaluated following the methodology of Cliquet *et al.* [46] for evaluating the boundary-layer thickness and external-flow velocity. Both edge-search and integrations are performed along the quasi-wall-normal structured-grid lines. The threshold values $\epsilon_\Omega = 0.0005$ and $\epsilon_\tau = 0.00005$ were used in the present applications.

2. Roberts correlation [43]

Transition onset, s_{tr}, in the LSB is given by [43]

$$\frac{s_{\mathrm{tr}} - s_{\mathrm{sep}}}{\theta_{\mathrm{sep}}} = \frac{25000}{Re_{\theta_{\mathrm{sep}}}} \log_{10}\left[\coth\left(10\max(0.001, T_u)\left(\frac{c}{L_s}\right)^{\frac{1}{5}}\right)\right] \tag{11}$$

where s_{sep} is the location of the laminar separation point, T_u is the external flow turbulence intensity (bounded above 0.1%) and L_s the longitudinal integral lengthscale [43]. In the absence of data for L_s, $L_s = c/15.8$ was taken in the applications.

3. AHD-Gleyzes criterion

The Arnal-Habiballah-Delcourt [44, 69, 70] (AHD) criterion is used jointly with the Gleyzes [45] criterion for the natural attached and separated transition onset computation of the boundary-layer. Details on the formulation, implementation and use can be found in [46, 66]. The AHD criterion is expressed as follows:

$$Re_{\theta tr} = -206\exp(25.7\overline{\Lambda_2})[\ln(16.8T_u) - 2.77\overline{\Lambda_2}] + Re_{\theta cr} \tag{12}$$

The transition onset is located at the point $s = s_{tr}$ when $Re_{\theta(s)} = Re_{\theta tr}$ is reached. The subscript "*cr*" denotes the critical point, which is located at $s = s_{cr} < s_{tr}$ when $Re_{\theta(s)} = Re_{\theta cr} = \exp(52/H_{(s)} - 14.8)$. The mean Pohlhausen parameter $\overline{\Lambda_2}$ is expressed as:

$$\overline{\Lambda_2} = \frac{1}{s - s_{cr}} \int_{s_{cr}}^{s} \frac{-\theta^2}{\mu U_e} \frac{\partial p_{wall}}{\partial s} \mathrm{d}s \tag{13}$$

Where U_e denotes the magnitude of the velocity at the boundary-layer edge and p_{wall} the pressure at the wall.

If the shape parameter reaches the value $H_{(s=s_{sw})} = H_{sw} = 2.8$, and transition onset has not been reached ($Re_{\theta(s=s_{sw})} = Re_{\theta sw} < Re_{\theta tr}$; *switch* point $s = s_{sw}$), the Gleyzes criterion is applied for $s > s_{sw}$. The start value of the total amplification factor N_{sw} is computed by injecting the Mack's relationship [67], $N = -2.4\ln(T_u) - 8.43$, into eqn. (12) and solving for N at the point

$s = s_{sw}$. Then, the Gleyzes criterion can be evaluated for $s > s_{sw}$, which is better adapted to high values of H than the AHD criterion

$$N_{(s)} = N_{sw} + \int_{Re_{\theta sw}}^{Re_\theta} \frac{-2.4}{\mathcal{B}_{GL}} \mathrm{d}Re_\theta \tag{14}$$

Where $\mathcal{B}_{GL}$ is the *Gleyzes function* and is expressed as follows

$$\mathcal{B}_{GL} = \begin{cases} \dfrac{-162.11093}{H^{1.1}} & \text{for} \quad 3.36 < H \\ -73[\exp\left[-1.56486(H-3.02)\right]] & \text{for} \quad 2.8 < H \leq 3.36 \\ -103[\exp[-4.12633(H-2.8)]] & \text{else} \end{cases} \tag{15}$$

The transition onset is located at the point $s = s_{tr}$ such that $N_{(s=s_{tr})}$ of eqn. (14) is equal to a critical total amplification factor N_{cr} related to the external turbulence level. We note that this transitional total amplification factor can be deduced from a characteristic external turbulence rate via the Mack relationship [67].

Acknowledgments

The authors would like to acknowledge the great support and useful insights of our colleges at the DAAA and DMPE Departments at ONERA. The simulations run in this study have been executed using the software elsA, which is issued of the three-party agreement between AIRBUS, SAFRAN, and ONERA. This work has been completely funded by ONERA.

References

[1] Tani, I., "Low-speed flows involving bubble separations," *Progress in Aerospace Sciences*, Vol. 5, 1964, pp. 70 – 103,
doi:10.1016/0376-0421(64)90004-1.

[2] Richez, F., Mary, I., Gleize, V., and Basdevant, C., "Near stall simulation of the flow around an airfoil using zonal RANS/LES coupling method," *Computers & Fluids*, Vol. 37, No. 7, 2008, pp. 857 – 866, doi:10.1016/j.compfluid.2007.03.016.

[3] Raffel, M., Favier, D., Berton, E., Rondot, C., Nsimba, M., and Geissler, W., "Micro-PIV and ELDV wind tunnel investigations of the laminar separation bubble above a helicopter blade tip," in "6th

International Symposium on Particle Image Velocimetry," Pasadena, California, USA, Vol. 17, 2005, pp. 1–13,
doi:10.1088/0957-0233/17/7/003.

[4] Pines, D. J. and Bohorquez, F., "Challenges Facing Future Micro-Air-Vehicle Development," *Journal of Aircraft*, Vol. 43, No. 2, 2006, pp. 290–305,
doi:10.2514/1.4922.

[5] Somers, D. M., "Design and Experimental Results for the S809 Airfoil," Tech. Rep. NREL/SR-440-6918, National Renewable Energy Laboratory, Golden, Colorado, USA, 1997.

[6] Gaster, M., "The Structure and Behaviour of Laminar Separation Bubbles," Tech. Rep. R&M No. 3595, Aeronautical Research Council, 1969.

[7] Malkiel, E. and Mayle, R. E., "Transition in a Separation Bubble," *Journal of Turbomachinery*, Vol. 118, No. 4, 1996, pp. 1–11,
doi:10.1115/1.2840931.

[8] Hain, R., Kähler, C. J., and Radespiel, R., "Dynamics of laminar separation bubbles at low-Reynolds-number aerofoils," *Journal of Fluid Mechanics*, Vol. 630, 2009, pp. 129–153,
doi:10.1017/S0022112009006661.

[9] Crabtree, L., "The Formation of Regions of Separated Flow on Wing Surfaces," Tech. Rep. 3122, ARC R&M, London, 1959.

[10] Sanz, W. and Platzer, M. F., "On the Navier-Stokes Calculation of Separation Bubbles With a New Transition Model," *Journal of Turbomachinery*, Vol. 120, No. 1, 1998, pp. 36–42,
doi:10.1115/1.2841385.

[11] Horton, H. P., *Laminar separation bubbles in two- and three-dimensional incompressible flow*, Ph.D. thesis, University of London, 1968.

[12] Carmichael, B., "Low Reynolds number airfoil survey," Tech. Rep. NASA-CR-165803, NASA, 1982.

[13] Jones, L. E., Sandberg, R. D., and Sandham, N. D., "Direct numerical simulations of forced and unforced separation bubbles on an airfoil at incidence," *Journal of Fluid Mechanics*, Vol. 602, 2008, pp. 175–207,
doi:10.1017/S0022112008000864.

[14] Yarusevych, S. and Kotsonis, M., "Steady and transient response of a laminar separation bubble to controlled disturbances," *Journal of Fluid Mechanics*, Vol. 813, 2017, pp. 955–990,
doi:10.1017/jfm.2016.848.

[15] Michelis, T., Yarusevych, S., and Kotsonis, M., "On the origin of spanwise vortex deformations in laminar separation bubbles," *Journal of Fluid Mechanics*, Vol. 841, 2018, pp. 81–108,

doi:10.1017/jfm.2018.91.

[16] Dick, E. and Kubacki, S., "Transition models for turbomachinery boundary layer flows : a review," *International Journal Of Turbomachinery Propulsion And Power*, Vol. 2, No. 2, 2017, p. 44.

[17] Langtry, R. B., Menter, F. R., Likki, S. R., Suzen, Y. B., Huang, P. G., and Völker, S., "A Correlation-Based Transition Model Using Local Variables - Part II: Test Cases and Industrial Applications," *Journal of Turbomachinery*, Vol. 128, 2006, pp. 423–434,
doi:10.1115/1.2184353.

[18] Langtry, R. B. and Menter, F. R., "Correlation-Based Transition Modeling for Unstructured Parallelized Computational Fluid Dynamics Codes," *AIAA Journal*, Vol. 47, No. 2, 2009, pp. 2894–2906,
doi:10.2514/1.42362.

[19] Abu-Ghannam, B. J. and Shaw, R., "Natural transition of boundary-layers – The effects of turbulence, pressure gradient, and flow history," *IMechE J. Mech. Eng. Sci.*, Vol. 22, No. 5, 1980, pp. 213–228,
doi:10.1243/JMES_JOUR_1980_022_043_02.

[20] Dhawan, S. and Narasimha, R., "Some properties of boundary layer flow during the transition from laminar to turbulent motion," *Journal of Fluid Mechanics*, Vol. 3, No. 4, 1958, pp. 418–436,
doi:10.1017/S0022112058000094.

[21] Durbin, P., "An intermittency model for bypass transition," *International Journal of Heat and Fluid Flow*, Vol. 36, 2012, pp. 1–6,
doi:10.1016/j.ijheatfluidflow.2012.03.001.

[22] Menter, F. R., Smirnov, P. E., Liu, T., and Avancha, R., "A One-Equation Local Correlation-Based Transition Model," *Flow, Turbulence and Combustion*, Vol. 95, No. 4, 2015, pp. 583–619,
doi:10.1007/s10494-015-9622-4.

[23] Walters, D. K. and Leylek, J. H., "A New Model for Boundary Layer Transition Using a Single-Point RANS Approach," *Journal of Turbomachinery*, Vol. 126, No. 1, 2004, pp. 193–202,
doi:10.1115/1.1622709.

[24] Walters, D. K. and Leylek, J. H., "Computational Fluid Dynamics Study of Wake-Induced Transition on a Compressor-Like Flat Plate," *Journal of Turbomachinery*, Vol. 127, No. 1, 2005, pp. 52–63,
doi:10.1115/1.1791650.

[25] Walters and Cokljat, "A Three-Equation Eddy-Viscosity Model for Reynolds-Averaged Navier-Stokes Simulations of Transitional Flow," *Journal of Fluids Engineering*, Vol. 130, No. 12,
doi:10.1115/1.2979230.

[26] Mayle, R. E. and Schulz, A., "The path to predicting bypass transition," *ASME J. Turbom.*, Vol. 119,

1997, pp. 405–411,
doi:10.1115/1.2841139.

[27] Tani, I., "Boundary-later transition," *Ann. Rev. Fluid Mech.*, Vol. 1, 1969, pp. 169–196.

[28] Gerolymos, G. A. and Vallet, I., "The dissipation tensor ε_{ij} in wall turbulence," *J. Fluid Mech.*, Vol. 807, 2016, pp. 386–418,
doi:10.1017/jfm.2016.610.

[29] Kubacki, S. and Dick, E., "An algebraic intermittency model for bypass, separation-induced and wake-induced transition," *International Journal of Heat and Fluid Flow*, Vol. 62, 2016, pp. 344–361,
doi:10.1016/j.ijheatfluidflow.2016.09.013.

[30] Minot, A., Salah El-Din, I., Barrier, R., Boniface, J. C., and Marty, I., "Improvement of Laminar-Turbulent Transition Modeling Within a Low-Pressure Turbine," in "ASME Turbo Expo 2016: Turbomachinery Technical Conference and Exposition," ASME, Seoul, South Korea, Vol. 2C, 2016,
doi:10.1115/GT2016-57637.

[31] Colonia, S., Leble, V., Steijl, R., and Barakos, G., "Assessment and Calibration of the γ-Equation Transtion Model at Low Mach," *AIAA Journal*, Vol. 55, No. 4, 2017, pp. 1126–1139,
doi:10.2514/1.J055403.

[32] de Rosa, D. and Catalano, P., "Validation of Intermittency Model for Transition Prediction in a RANS Flow Solver," in "AIAA Aerospace Sciences Meeting," AIAA, 2018,
doi:10.2514/6.2018-1043.

[33] Yuan, W., Khalid, M., Windte, J., Scholz, U., and Radespiel, R., "An Investigation of Low-Reynolds-Number Flows past Airfoils," in "23rd AIAA Applied Aerodynamics Conference," Toronto, AIAA-2005-4607, 2005,
doi:10.2514/6.2005-4607.

[34] Windte, J., Scholz, U., and Radespiel, R., "Validation of the RANS-simulation of laminar separation bubbles on airfoils," *Aerospace Science and Technology*, Vol. 10, No. 6, 2006, pp. 484–494,
doi:10.1016/j.ast.2006.03.008.

[35] Menter, F. R., "Two-equation eddy-viscosity turbulence models for engineering applications," *AIAA Journal*, Vol. 32, No. 8, 1994, pp. 1598–1605,
doi:10.2514/3.12149.

[36] Lian, Y. and Shyy, W., "Laminar-Turbulent Transition of a Low Reynolds Number Rigid or Flexible Airfoil," *AIAA Journal*, Vol. 45, No. 7, 2007, pp. 1501–1513,
doi:10.2514/1.25812.

[37] Wilcox, D. C., "Simulation of Transition with a Two-Equation Turbulence Model," *AIAA Journal*, Vol. 32, No. 2, 1994, pp. 247–255,
doi:10.2514/3.59994.

[38] Smith, A. and Gamberoni, N., *Transition, Pressure Gradient and Stability Theory*, Douglas Aircraft Company, El Segundo Division, 1956.

[39] Catalano, P. and Tognaccini, R., "Turbulence Modeling for Low-Reynolds-Number Flows," *AIAA Journal*, Vol. 48, No. 8, 2010, pp. 1673–1685,
doi:10.2514/1.J050067.

[40] Catalano, P., Mele, B., and Tognaccini, R., "A Numerical Method to Detect Laminar Separation Bubbles over Airfoils," in "31st AIAA Applied Aerodynamics Conference," AIAA, San Diego, CA, USA, 2013,
doi:10.2514/6.2013-2528.

[41] Wilcox, D. C., *Turbulence Modeling for CFD*, DCW Industries, La Cañada, California, 3rd ed., 2006.

[42] Wilcox, D. C., "A Half Century Historical Review of the k-ω Model," in AIAA, ed., "29th Aerospace Sciences Meeting," Reno, Nevada, 1991,
doi:10.2514/6.1991-615.

[43] Roberts, W. B., "Calculation of Laminar Separation Bubbles and Their Effect on Airfoil Performance," *AAIA Journal*, Vol. 18, No. 1, 1980, pp. 25–31.

[44] Arnal, D., Habiballah, M., and Coustols, E., "Laminar Instability Theory And Transition Criteria In Two and Three-Dimensional Flow," *Recherche Aérospatiale*, Vol. 2, 1984, pp. 125–143.

[45] Gleyzes, C., Cousteix, J., and Bonnet, J., *Numerical and Physical Aspects of Aerodynamic Flows II*, Springer-Verlag, New York, chap. Calculation method of leading edge separation bubbles, pp. 173–192, 1984.

[46] Cliquet, J., Houdeville, R., and Arnal, D., "Application of Laminar-Turbulent Transition Criteria in Navier-Stokes Computations," *AIAA Journal*, Vol. 46, No. 5, 2008, pp. 1182–1190,
doi:10.2514/1.30215.

[47] Laurent, C., Mary, I., Gleize, V., Lerat, A., and Arnal, D., "RANS Modeling of a Transitional Laminar Separation Bubble on a Flat Plate with DNS Database," AIAA, Chicago, Illinois, 2010,
doi:10.2514/6.2010-4444.

[48] Laurent, C., Mary, I., Gleize, V., Lerat, A., and Arnal, D., "DNS database of a transitional separation bubble on a flat plate and application to RANS modeling validation," *Computers & Fluids*, Vol. 61, 2012, pp. 21 – 30,
doi:10.1016/j.compfluid.2011.07.011. Onera Scientific Day.

[49] Arnal, D., "Laminar-turbulent transition problems in supersonic and hypersonic flow," Tech. Rep. 761, AGARD, 1988.

[50] Richez, F., Mary, I., Gleize, V., and Basdevant, C., *Simulation and Modelling of a Laminar Separation Bubble on Airfoils*, Springer Netherlands, Dordrecht, pp. 457–469, 2009, doi:10.1007/978-1-4020-9898-7_39.

[51] Alam, M. and Sandham, N. D., "Direct numerical simulation of short laminar separation bubbles with turbulent reattachment," *Journal of Fluid Mechanics*, Vol. 410, 2000, pp. 1–28.

[52] Spalart, P. and Strelets, M., "Mechanisms of transition and heat transfer in a separation bubble," *Journal of Fluid Mechanics*, Vol. 403, 2000, pp. 329–349.

[53] Spalart, P. R., "Direct simulation of a turbulent boundary layer up to Re_θ=1410," *Journal of Fluid Mechanics*, Vol. 187, 1988, pp. 61–98, doi:10.1017/S0022112088000345.

[54] Menter, F. R., Langtry, R. B., Likki, S. R., Suzen, Y. B., Huang, P. G., and Völker, S., "A Correlation-Based Transition Model Using Local Variables - Part I: Model Formulation," *Journal of Turbomachinery*, Vol. 128, 2006, pp. 413–422, doi:10.1115/1.2184352.

[55] Minot, A., de Saint Victor, X., Marty, J., and Perraud, J., "Advanced Numerical Setup for Separation-Induced Transition on High-Lift Low-Pressure Turbine Flows Using the γ-$\widetilde{Re_\theta}$ Model," in "ASME turbo Expo," Montreal, Canada, 2015.

[56] Wilcox, D. C., "Formulation of the k-ω Turbulence Model Revisited," *AIAA Journal*, Vol. 46, No. 11, 2008, pp. 2823–2838, doi:10.2514/1.36541.

[57] Cambier, L., Heib, S., and Plot, S., "The Onera elsA CFD software: input from research and feedback from industry," *Mechanics & Industry*, Vol. 14, No. 3, 2013, pp. 159–174, doi:10.1051/meca/2013056.

[58] Morkovin, M., "Effects of Compressibility on Turbulent Flows," in Favre, A., ed., "Mecanique de la Turbulence," Gordon and Breach, New York, pp. 367–380, 1962.

[59] Wilcox, D. C., "Reassessment of the scale-determining equation for advanced turbulence models," *AIAA Journal*, Vol. 26, No. 11, 1988, pp. 1299–1310, doi:10.2514/3.10041.

[60] Kok, J., "Resolving the Dependence on Freestream Values for the k- Turbulence Model," *AIAA Journal*, Vol. 38, No. 7, 2000, pp. 1292–1295,

doi:10.2514/2.1101.

[61] Menter, F. R., "Performance of popular turbulence model for attached and separated adverse pressure gradient flows," *AIAA Journal*, Vol. 30, No. 8, 1992, pp. 2066–2072, doi:10.2514/3.11180.

[62] Benoit, C., Péron, S., and Landier, S., "Cassiopee: A CFD pre- and post-processing tool," *Aerospace Science and Technology*, Vol. 45, No. Supplement C, 2015, pp. 272 – 283, doi:10.1016/j.ast.2015.05.023.

[63] Rumsey, C. L., "Apparent transition behavior of widely-used turbulence models," *International Journal of Heat and Fluid Flow*, Vol. 28, No. 6, 2007, pp. 1460–1471, doi:10.1016/j.ijheatfluidflow.2007.04.003.

[64] Spalart, P. and Rumsey, C. L., "Effective Inflow Conditions for Turbulence Models in Aerodynamic Calculations," *AIAA Journal*, Vol. 45, No. 10, 2007, pp. 2544–2553, doi:10.2514/1.29373.

[65] Bernardos, L., Richez, F., Gleize, V., and Gerolymos, G. A., "On the k-ω models behavior in the boundary-layer downstream of a short transitional separation bubble," in "AIAA Aerospace Sciences Meeting," AIAA, Kissimmee, Florida, USA, 2018, doi:10.2514/6.2018-0376.

[66] Perraud, J., Deniau, H., and Casalis, G., "Overview Of Transition Prediction Tools In The elsA Software," in "6th European Conference on Computational Fluid Dynamics," Barcelona, Spain, 2014.

[67] Mack, L. M., "Transition prediction and linear stability theory," Tech. Rep. CP 224, 1.1-1.22, AGARD, 1977.

[68] Alferez, N., Mary, I., and Lamballais, E., "Study of Stall Development Around an Airfoil by Means of High Fidelity Large Eddy Simulation," *Flow, Turbulence and Combustion*, Vol. 91, No. 3, 2013, pp. 623–641, doi:10.1007/s10494-013-9483-7.

[69] Arnal, D., "Description and Prediction of Transition in Two-Dimensional Incompressible Flow," in "Special Course on Stability and Transition of Laminar Flow," NATO-AGARD, 709, chap. 2, 1984.

[70] Arnal, D., "Boundary Layer Transition: Predictions Based on Linear Theory," in "Special Course on Progress in Transition Modelling," AGARD, 793, chap. 2, pp. 1–63, 1994.